Cold-responsive adipocyte progenitors couple adrenergic signaling to immune cell activation to promote beige adipocyte accrual

Bo Shan,[1] Mengle Shao,[1] Qianbin Zhang, Yu A. An, Lavanya Vishvanath, and Rana K. Gupta

Touchstone Diabetes Center, Department of Internal Medicine, University of Texas Southwestern Medical Center, Dallas, Texas 75390, USA

The full array of cold-responsive cell types within white adipose tissue that drive thermogenic beige adipocyte biogenesis remains undefined. We demonstrate that acute cold challenge elicits striking transcriptomic changes specifically within DPP4+ PDGFRβ+ adipocyte precursor cells, including a β-adrenergic receptor CREB-mediated induction in the expression of the prothermogenic cytokine, *Il33*. Doxycycline-inducible deletion of *Il33* in PDGFRβ+ cells at the onset of cold exposure attenuates ILC2 accumulation and beige adipocyte accrual. These studies highlight the multifaceted roles for adipocyte progenitors and the ability of select mesenchymal subpopulations to relay neuronal signals to tissue-resident immune cells in order to regulate tissue plasticity.

Supplemental material is available for this article.

Received June 20, 2021; revised version accepted September 2, 2021.

The adaptation to cold environmental temperatures involves remodeling of energy-storing white adipose tissue (WAT) into a thermogenic energy-burning phenotype reminiscent of brown adipose tissue (BAT) (Lončar 1991). This "browning" of WAT is classically defined by the emergence of multilocular UCP1+ beige adipocytes, which have the ability to increase energy expenditure and improve nutrient homeostasis when fully active (Cohen and Kajimura 2021). Thermogenic WAT remodeling is triggered by β-adrenergic (βAR) signaling and involves notable alterations in the immune cell composition of the tissue microenvironment (Shamsi et al. 2021). The full array of cold-responsive cell types in WAT that drive this thermogenic tissue remodeling remains undefined.

Murine inguinal iWAT (iWAT) harbors hierarchical mesenchymal adipocyte precursor cell (APC) subpopulations (Burl et al. 2018; Schwalie et al. 2018; Merrick et al. 2019; Shao et al. 2021). Two distinct subpopulations of PDGFRβ+ APCs can be separated and isolated based on expression of dipeptidyl peptidase 4 protein (DPP4). DPP4+ APCs represent multipotent mesenchymal progenitors, whereas DPP4− APCs are further differentiated and represent committed preadipocytes (Merrick et al. 2019). PDGFRβ+ APCs undergo beige adipocyte differentiation after prolonged cold exposure (2 wk at 6°C); however, during the first week of cold challenge, PDGFRβ+ APCs do not appear to give rise to appreciable amounts of beige adipocytes (Vishvanath et al. 2016). Here, we tested the hypothesis that APCs contribute to the early stages of thermogenic iWAT remodeling independent of their intrinsic differentiation capacity. We found that DPP4+ APCs represent the principal source of the prothermogenic cytokine, IL-33, in iWAT, and that *Il33* expression in APCs is driven directly by the βAR-CREB signaling cascade. These data identify a select subpopulation of iWAT APCs that is uniquely cold-responsive and serves to couple adrenergic signaling to immune cell activation to facilitate the early stages of cold-induced thermogenic remodeling.

Results and Discussion

We hypothesized that APCs contribute to the early stages of thermogenic iWAT remodeling independent of their capacity to undergo adipocyte differentiation. To test this, we first isolated DPP4+ and DPP4− APCs from male wild-type C57BL/6 mice housed for 1 d at 6°C and immediately performed bulk RNA sequencing (Supplemental Fig. S1A). Principal component analysis and unbiased hierarchical sample clustering revealed that DPP4+ APCs from cold-exposed animals were strikingly distinct from DPP4+ APCs isolated from mice maintained at room temperature (Fig. 1A; Supplemental Fig. S2A). Cold exposure led to significant changes in expression of 1277 genes in DPP4+ APCs (fold change > 2; P-value < 0.01) (Supplemental Data Set 1). Remarkably, DPP4− committed APCs from cold-exposed mice could not be distinguished from DPP4− APCs from mice maintained at room temperature (Fig. 1A; Supplemental Fig. S2A) and far fewer significant changes in gene expression were observed in this subpopulation after cold exposure (Supplemental Data Set 2). Gene set enrichment analysis identified an enrichment in mRNA signatures of cell proliferation in DPP4+ APCs following cold exposure (Supplemental Data Set 3). Indeed, we observed that cold exposure led to an increase in the numbers of DPP4+ APCs, but not DPP4− APCs (Supplemental Fig. S2B). In vitro, both DPP4+ and DPP4− APCs are responsive to the addition of the β-adrenergic receptor agonist, isoproterenol (Supplemental Fig. S2C); however, there are significant differences in how these subpopulations are impacted (Supplemental Fig. S2C). Most of the genes whose expression levels are elevated in DPP4+ APCs upon isoproterenol treatment are only modestly elevated, or unchanged, in DPP4− APCs (Supplemental Fig. S2C). These data indicate that APC subpopulations differentially respond to cold challenge in vivo and β-adrenergic receptor activation in vitro.

[*Keywords*: CREB; ILC2; Il33; adipocyte progenitors; adrenergic signaling; beige adipocytes; cold exposure]

[1]**These authors contributed equally to this work.**

Corresponding author: rana.gupta@utsouthwestern.edu

Article published online ahead of print. Article and publication date are online at http://www.genesdev.org/cgi/doi/10.1101/gad.348762.121.

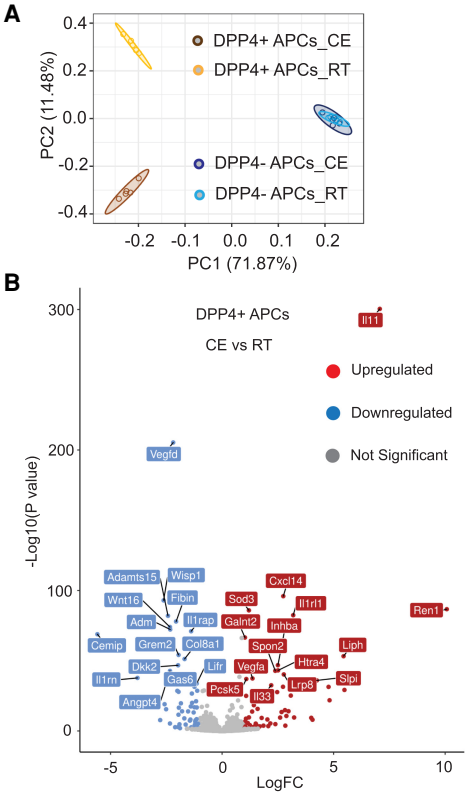

Figure 1. Transcriptomic changes in DPP4+ APCs following acute cold exposure. (*A*) Principal component analysis (PCA) of transcriptomic data obtained by bulk RNA-seq of DPP4+ PDGFRβ+ cells and DPP4− PDGFRβ+ cells isolated from iWAT of animals maintained at room temperature (22°C) or cold-exposed (CE; 6°C) for 1 day. $n = 5$ for each group. Each sample (n) represents cells pooled from two mice. (*B*) Volcano plot depicting the top 15 up-regulated and top 15 down-regulated genes in cold-exposed DPP4+ cells that encode predicted secreted proteins. See Supplemental Data Set S4.

Adipose progenitors have the capacity to release secreted factors into the tissue microenvironment (Mahlakõiv et al. 2019; Rana et al. 2019; Spallanzani et al. 2019; Shan et al. 2020). Thus, we identified genes encoding putative secreted proteins among the list of genes regulated by cold exposure in DPP4+ APCs (Fig. 1B; Supplemental Data Set 4). qPCR analysis of the most differentially regulated genes in DPP4+ cells confirmed their regulation by cold exposure (Supplemental Fig. S3A,B). Particularly noteworthy was the selective expression and regulation of *Il33* in DPP4+ APCs. Interleukin-33 (IL33) is a member of the IL-1 receptor superfamily of cytokines. Studies of global *Il33* knockout mice revealed that IL-33 is required during the perinatal period for proper *Ucp1* mRNA splicing and effective BAT function (Odegaard et al. 2016). In adult animals, exogenous IL-33 promotes iWAT thermogenic remodeling through the activation of ILC2s (Brestoff et al. 2015; Lee et al. 2015). ILC2s produce methionine–enkephalin (MetENK) peptides that act directly on adipocytes to activate *Ucp1* and promote the emergence of thermogenic beige adipocytes (Brestoff et al. 2015). ILC2s also produce type 2 cytokines (e.g., IL-5 and IL-13) that stimulate the activation of eosinophils and alternatively activated macrophages to promote the browning of iWAT (Qiu et al. 2014; Lee et al. 2015).

The precise cellular source of *Il33* is tissue-dependent and includes both epithelial and mesenchymal cell types (Molofsky et al. 2015). In gonadal WAT, both mesothelial cells and a subset of perivascular mesenchymal cells represent principal sources of *Il33* expression (Mahlakõiv et al. 2019; Spallanzani et al. 2019). In iWAT, *Il33* expression has only been pinpointed to a broad pool of stromal cells (Lee et al. 2015; Rana et al. 2019). The identity of the precise stromal subpopulations that express *Il33* in this depot has not been resolved and mechanisms controlling its expression have not been fully defined. We observed that *Il33* is expressed at much higher levels within DPP4+ APCs than observed in DPP4− APCs (Fig. 2A). Further analysis indicated that the main isoform of *Il33* mRNA expressed in DPP4+ cells is *Il33a* rather than *Il33b* (Supplemental Fig. S4A). IL-33 protein expression is also selective to the DPP4+ APC subpopulation (Fig. 2B; Supplemental Fig. S4B). Indirect immunofluorescence assays revealed the presence of IL-33+ cells within the iWAT vasculature, consistent with the known localization of PDGFRβ+ perivascular APCs (Supplemental Fig. S5A). Moreover, we observed IL-33+ cells within the connective tissue surrounding the iWAT depot (reticular interstitium), a known region where DPP4+ APCs also

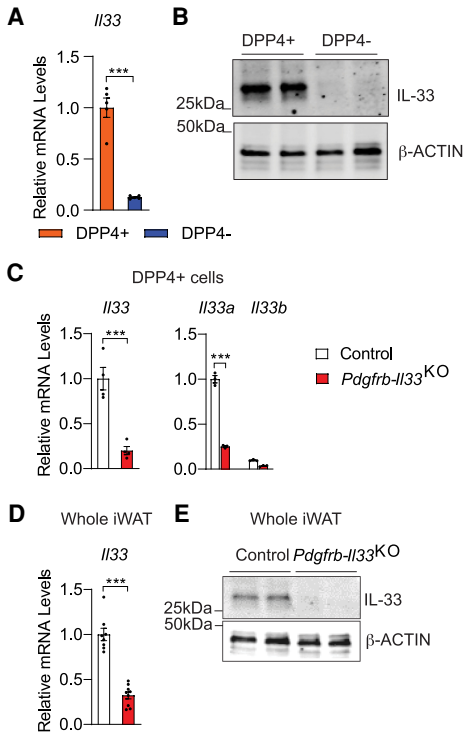

Figure 2. DPP4+ APCs are the principal source of *Il33* expression in iWAT. (*A*) mRNA levels of *Il33* in freshly sorted APCs ($n = 5$). (*B*) IL-33 expression in cultured APCs. β-ACTIN levels were used as loading controls. Each lane represents one cell lysate derived from pooled cells from four mice. (*C*) mRNA levels of *Il33* and individual *Il33* isoforms (*Il33a* and *Il33b*) in freshly sorted DPP4+ APCs from iWAT of control and *Pdgfrb-Il33*^{KO} mice after doxycycline-containing chow diet feeding ($n = 4$). (*D*) *Il33* expression in whole iWAT of control and *Pdgfrb-Il33*^{KO} mice after doxycycline-containing chow diet feeding ($n = 8$ for control; $n = 9$ for *Pdgfrb-Il33*^{KO}). (*E*) IL-33 levels in whole iWAT of control and *Pdgfrb-Il33*^{KO} mice after doxycycline-containing chow diet feeding. Bars represent mean + SEM. (***) $P < 0.001$ by two-tailed unpaired Student's *t*-test.

reside (Supplemental Fig. S5B; Merrick et al. 2019). We used flow cytometry and *Il33*-driven EGFP reporter mice to examine the selectivity of *Il33* promoter activity. Approximately 79% of DPP4+ PDGFRβ+ cells are EGFP+ whereas only ~6% of DPP4− PDGFRβ+ cells express EGFP (Supplemental Fig. S4C). Importantly, >96% of EGFP+ cells in iWAT are DPP4+ PDGFRβ+ cells, suggesting that this subpopulation of APCs represents the predominant source of IL-33 expression in this depot (Supplemental Fig. S4D). We tested this genetically using an inducible mouse model in which *Il33* is inactivated specifically in *Pdgfrb*-expressing cells in a doxycycline (Dox)-inducible manner (*Pdgfrb*^{rtTA}; *TRE-CRE*; *Il33*$^{loxP/loxP}$ mice; referred to here as "*Pdgfrb-Il33*^{KO}" mice). Two weeks of Dox-containing chow diet feeding led to a >75% reduction in *Il33* mRNA levels within PDGFRβ+ cells (Fig. 2C). Importantly, *Il33* mRNA levels were reduced by the same degree when assayed across the whole depot (Fig. 2D). Moreover, IL-33 protein levels in whole-tissue lysates were barely detectable when in *Pdgfrb-Il33*^{KO} mice (Fig. 2E). These data reveal that DPP4+ APCs represent the principal site for *Il33* expression within the iWAT depot of adult mice under homeostatic conditions.

One day of cold exposure induced *Il33* expression in DPP4+ APCs (Fig. 1B). *Il33* expression in DPP4+ cells peaked at 1 d of cold exposure and then began to decline, with *Il33a* remaining the most abundant of the two isoforms (Fig. 3A; Supplemental Fig. S6A). Over the period examined, *Il33* levels in committed DPP4− APCs remained low. *Il33*-driven GFP expression was also selective to DPP4+ APCs after 1 d of cold exposure (Fig. 3B). At 2 d of cold exposure, we detected an increase in the protein levels of full-length IL-33 within whole iWAT (Supplemental Fig. S6B). The temporal pattern of *Il33* expression within DPP4+ APCs mimics the pattern of *Il33* expression observed when assayed across the whole depot (Fig. 3C). Tissue levels of *Il13*, a surrogate for ILC2 activation, also followed the same temporal pattern following cold exposure (Fig. 3C). In fact, the frequency of ILC2s in iWAT also began to increase after 1 d of cold exposure, coincident with the increase in *Il33* expression in DPP4+ APCs (Fig. 3D). We asked whether *Il33* expression in DPP4+ APCs is impacted by higher ambient temperature. Adult mice raised at 22°C were moved into 30°C housing chambers for 6 wk. As expected, thermoneutral housing leads to strong reduction in iWAT *Ucp1* expression (Supplemental Fig. S6C). This correlates with a reduction in *Il33* levels in whole tissue and selectively within DPP4+ APCs (Supplemental Fig. S6C,D). These data highlight the temperature sensitivity of DPP4+ APCs and the physiological regulation of *Il33* expression within this specific stromal subpopulation.

βAR signaling is the principal driver of thermogenic WAT remodeling; therefore, we tested whether *Il33* gene expression within DPP4+ APCs is regulated by this pathway. One injection of the βAR agonist, isoproterenol, led to an increase in tissue levels of *Il33*, coinciding with an increase in *Il33* expression selectively within DPP4+ APCs (Supplemental Fig. S7A,B). Isoproterenol can induce *Il33* expression in DPP4+ APCs in a cell-autonomous manner. Treatment of cultured DPP4+ APCs with isoproterenol leads to marked up-regulation of *Il33* mRNA levels, whereas the levels of *Il33* in isoproterenol-treated DPP4− APCs remain low (Supplemental Fig. S7C). IL-33 protein levels in DPP4+ cell lysates and conditioned medium were also robustly elevated in a time-dependent manner upon isoproterenol treatment (Supplemental Fig. S7D, E). Classical βAR signaling involves the activation of β1, β2, and/or β3 adrenergic receptors (AR), leading ultimately to PKA-mediated phosphorylation and activation of the transcription factor CREB. We found that both *Adrb1* (β1AR) and *Adrb2* (β2AR) are expressed in DPP4+ and DPP4− APCs, whereas *Adrb3* (β3AR) expression was relatively very low (Supplemental Fig. S7F). Notably, the β3AR-selective agonist, CL316,243, did not induce *Il33* expression (Supplemental Fig. S7C). This suggests that β1AR and/or β2AR are the principal mediators of isoproterenol in these cells. We defined the relative contribution of PKA signaling and β1AR and β2AR by treating DPP4+ APCs with isoproterenol in combination with selective inhibitors. The addition of a PKA inhibitor (H-89) or a β1/β2 blocker (propranolol) blocked isoproterenol-induced IL-33 (Supplemental Fig. S7G). Importantly, isoproterenol-mediated induction of IL-33 is blunted in the

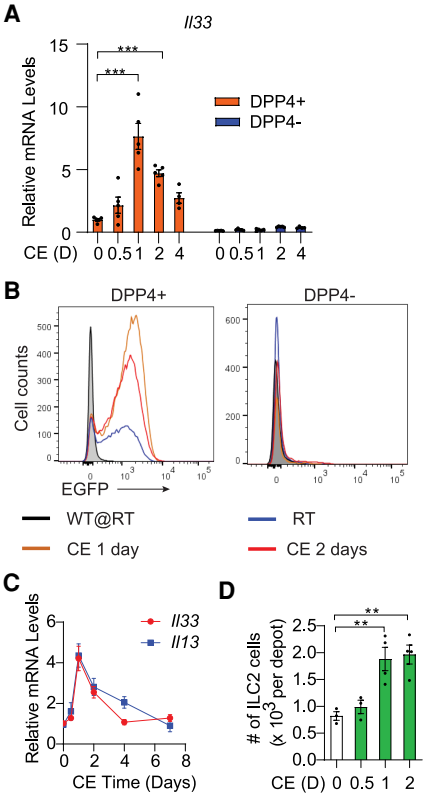

Figure 3. *Il33* expression in DPP4+ APCs is regulated upon acute cold exposure. (*A*) *Il33* expression in freshly sorted APCs isolated from adult iWAT depots at room temperature (D = 0) or the indicated days (D) following the onset of cold exposure (CE). $n = 5$ for 0-, 0.5-, 1-, 2-, and 4-d CE group, $n = 4$ for 7-d CE group. (*B*) Flow cytometry analysis of EGFP expression within APCs of iWAT depots from *Il33*-EGFP reporter mice maintained at room temperature (RT) or cold-exposed for 1 or 2 d. Room temperature-housed wild-type (WT) mice were used as negative control for EGFP expression. (*C*) mRNA levels of *Il33* and the ILC2-derived cytokine *Il13* in whole iWAT upon 0 (room temperature), 0.5, 1, 2, 4, and 7 d of cold exposure. $n = 6$ for each group. (*D*) ILC2 abundance in iWAT following 0 (room temperature), 0.5, 1, and 2 d of cold exposure. $n = 3$ for 0 and 0.5 d of cold exposure. $n = 4$ for 1 and 2 d of cold exposure. Bars represent mean + SEM. (**) $P < 0.01$, (***) $P < 0.001$ by one-way or two-way ANOVA.

presence of the β1 adrenergic receptor antagonist (CGP-20712A), more so than observed when the β2 adrenergic receptor antagonist (ICI-118551) is applied (Supplemental Fig. S7G). The data suggest that both receptors mediate this response; however, it appears that the β1AR is the principal mediator of isoproterenol-induced IL-33 expression in these cells.

ChIP-seq of phosphorylated CREB (p-CREB) occupancy in DPP4+ cells identified numerous genomic regions bound by CREB in an isoproterenol-dependent manner, including several elements in proximity to the *Il33* transcriptional start site (Fig. 4A). ChIP-PCR confirmed these findings and revealed that p-CREB or CREB occupancy at three elements containing putative CREB binding sites was enriched in DPP4+ APCs following isoproterenol treatment (Fig. 4B; Supplemental Figure S7H). This enrichment was much greater than observed in DPP4− APCs. *Creb* inactivation in DPP4+ APCs strongly suppressed the ability of isoproterenol to induce *Il33* expression (Fig. 4C,D). These data implicate the classical βAR-CREB signaling pathway as a direct regulator of *Il33* expression in DPP4+ APCs. Interestingly, isoproterenol induced p-CREB levels to a comparable degree in both DPP4+ and DPP4− APCs (Supplemental Fig. S7I). This suggests that the differential response of these two APC subpopulations is mediated by factors that control CREB occupancy at *Il33*, rather than CREB phosphorylation.

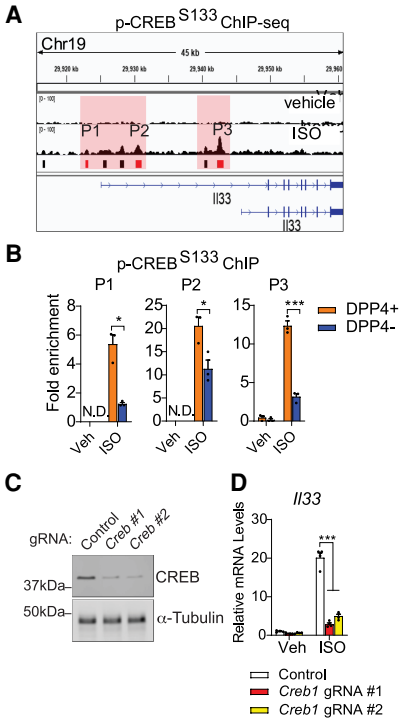

Figure 4. Isoproterenol induces *Il33* expression in DPP4+ APCs via CREB. (*A*) ChIP-seq analysis of phosphorylated CREB (S133; p-CREB) occupancy at the *Il33* locus in cultured DPP4+ APCs treated with isoproterenol or vehicle. Red boxes indicate bound regions (P1–P3) harboring predicted CREB response elements ("TGACGT/C"). Cells for ChIP-seq analysis were pooled from both iWAT depots of eight mice. (*B*) ChIP-PCR of pCREB occupancy at regions P1–P3 within cultured APCs following treatment with vehicle or isoproterenol. The cells were pooled from both iWAT depots of eight mice. (N.D.) Not detected. (*C*) CREB expression in DPP4+ APCs following CRISPR–Cas9-mediated inactivation of the *Creb* locus using independent gRNAs. Each lane represents lysates from cells pooled from both iWAT depots of four mice. (*D*) *Il33* expression in cultured DPP4+ APCs following treatment with vehicle or isoproterenol. $n = 4$ for each group. Bars represent mean + SEM. (*) $P < 0.05$, (***) $P < 0.001$ by two-way ANOVA.

Thermogenic iWAT remodeling in global/germline *Il33*-deficient mice is impaired (Mathis 2016; Odegaard et al. 2016); however, whether the observed cold-induced induction of endogenous stromal cell *Il33* expression is required for the initiation of thermogenic WAT remodeling in adult mice has been unclear. We administered 8-wk-old control (*Pdgfrb*^{rtTA}; *Il33*$^{loxP/loxP}$ mice) and *Pdgfrb-Il33*^{KO} mice Dox chow diet for 4 wk at room temperature to induce *Il33* deletion in PDGFRβ+ cells. Animals were then housed for 7 d at 6°C (Supplemental Fig. S8A). Cold exposure did not impact body weight in either control or *Pdgfrb-Il33*^{KO} mice (Supplemental Fig. S8B); however, cold exposure differentially impacted iWAT remodeling in these animals. In *Pdgfrb-Il33*^{KO} mice, we observed lower numbers of ILC2s along with lower tissue mRNA levels of ILC2-derived *Il13*, *Il5*, and *Penk* (encoding methionine–enkephalin) (Fig. 5A; Supplemental Fig. S8C). This coincides with lower tissue levels of key thermogenic genes, concomitant higher expression of white adipocyte-enriched transcripts, and slightly elevated expression of extracellular matrix components and inflammatory genes (Supplemental Fig. S8C–E). Notably, iWAT levels of UCP1 protein are markedly lower in *Pdgfrb-Il33*^{KO} mice than observed in controls (Fig. 5B). Analyses of cellular respiration using explanted whole tissues revealed reduced metabolic activity of iWAT from cold-exposed *Pdgfrb-Il33*^{KO} mice. Both baseline and FCCP-induced respiration are markedly lower in iWAT of cold-exposed *Pdgfrb-Il33*^{KO} mice as compared with controls (Fig. 5C). Moreover, we observed far fewer multilocular cells within iWAT of *Pdgfrb-Il33*^{KO} mice as compared with what is observed in iWAT from control mice (Fig. 5D). Notably, injection of MetENK during the cold exposure period at least partially restores thermogenic tissue remodeling in *Pdgfrb-Il33*^{KO} mice, supporting a role for this ILC2-derived peptide in IL33-mediated beige adipocyte formation (Fig. 5D; Supplemental Fig. S8F). Together, these data indicate that the ability to activate *Il33* expression in iWAT PDGFRβ+ cells at the onset of cold exposure is required for functional ILC2 activation and thermogenic remodeling of this tissue.

mRNA levels of the gene encoding interleukin 1 receptor-like 1 (ST2/IL1RL1), the IL-33 receptor, is induced in DPP4+ APCs upon cold exposure (Fig. 1B; Supplemental Data Set 1). This raises the possibility that IL-33 may function in a cell-autonomous manner. Importantly, *Il33* inactivation did not impact the intrinsic adipogenic capacity of DPP4+ APCs (Supplemental Fig. S8G,H). Moreover, prior lineage tracing studies suggest that beige cell recruitment occurring during this 7-d window of cold exposure does not depend on the de novo differentiation of *Pdgfrb*-expressing cells (Vishvanath et al. 2016). Thus, it is likely that IL-33 functions during this initial period of cold exposure in a manner independent of any ability to modulate the adipogenic capacity of PDGFRβ+ cells. Nevertheless, we cannot exclude the possibility that IL-33 from DPP4+ APCs acts in an autocrine manner after longer periods of cold exposure. Furthermore, we detected release of the full-length form of IL-33 from isoproterenol-treated DPP4+ APCs, coinciding with an increase in tissue levels of full-length IL-33 after cold exposure. The cleaved

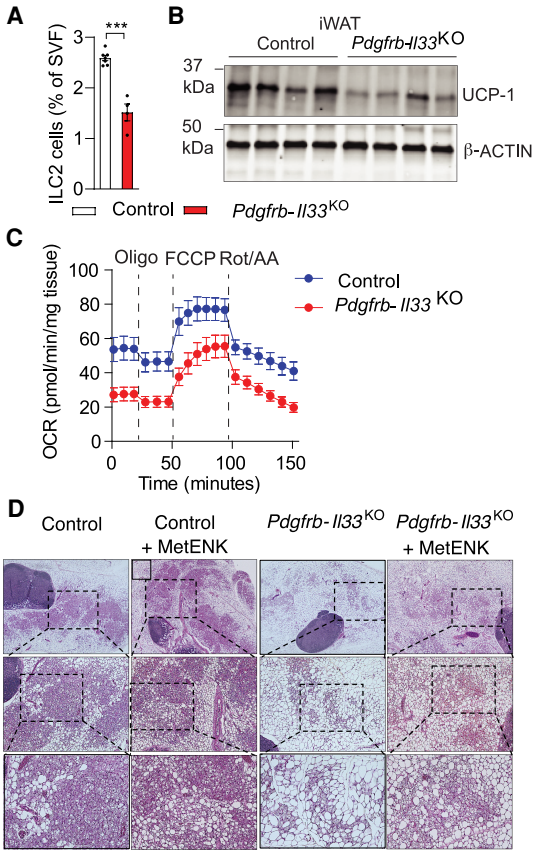

Figure 5. *Il33* inactivation in adult PDGFRβ+ cells impairs cold-induced iWAT remodeling. (*A*) ILC2 frequency following cold exposure. Control, $n = 7$; *Pdgfrb-Il33*^{KO}, $n = 4$. Bars represent mean + SEM. (***) $P < 0.001$ by two-tailed unpaired Student's *t*-test. (*B*) UCP-1 levels following cold exposure. β-ACTIN levels were used as loading controls. (*C*) Oxygen consumption of whole iWAT isolated following cold exposure. Control, $n = 7$; *Pdgfrb-Il33*^{KO}, $n = 10$. (*D*) iWAT H&E staining following cold exposure with or without Met-ENK or vehicle (PBS) treatment. (*Top* row) 4× magnification. (*Middle* row) 10× magnification of boxed regions in the *top* row. (*Bottom* row) 20× magnification of boxed regions in the *middle* row.

form of IL-33 is more active under certain conditions; however, the full-length form is reported to also be active and capable of activating ST2 (Lüthi et al. 2009). Additional studies will be needed to understand how IL-33 protein is released from cells under these conditions.

The phenotype of *Pdgfrb-Il33*^{KO} mice aligns well with the model proposed by Brestoff et al. (2015) They postulated that IL-33's critical function in cold-induced thermogenesis is to promote the accumulation of ILC2s, which mediate beige adipocyte biogenesis through the production of methionine-enkephalin peptides (Brestoff et al. 2015). Our data add to this model by indicating that cold-responsive DPP4+ APCs are the principal source of IL-33 in iWAT, and that β-adrenergic signaling acts directly on these cells to drive *Il33* expression via a CREB-dependent mechanism. As such, this distinct APC subpopulation serves to relay signals from the nervous system to immune cells in an effort to facilitate rapid adaptation to cold challenge. We show here at IL-33 represents one key factor derived from DPP4+ cells that affects thermogenic remodeling. Additional progenitor-derived factors that promote or inhibit the thermogenic plasticity of WAT in adults may exist. Unraveling the intercellular communication mediating these natural adaptions to cold challenge may reveal novel therapeutic strategies to promote beige adipocyte biogenesis and metabolic health in obesity.

Materials and methods

Study approval

Animal experiments were performed according to procedures approved by the University of Texas Southwestern Institutional Animal Care and Use Committee. The origins and descriptions of each strain and diet used are in the Supplemental Material.

Histology

H&E staining was performed on 4% paraformaldehyde-fixed paraffin-embedded tissues. Indirect immunofluorescence was performed as previously described (Shao et al. 2018). See the Supplemental Material for details regarding tissue fixation and antibodies.

Gene expression analysis

qPCR was performed as described (Hepler et al. 2018). See Supplemental Table S1 for primer sequences. Bulk RNA-seq libraries were assembled as described (Shan et al. 2020). See the Supplemental Material for additional details.

ChIP

ChIP was performed as described (Shan et al. 2020). DPP4+ APCs were treated with 10 µM isoproterenol (Sigma I6504) for 4 h prior to cross-linking. Details regarding antibodies, library preparation, and ChIP-seq analysis are in the Supplemental Material.

Western blotting

Protein extracts from cultured cells or tissues were prepared by homogenization in RIPA lysis buffer and resolved by SDS-PAGE. Primary antibodies were incubated with membranes at 4°C, and IR dye-coupled secondary antibodies (LI-COR) were used for visualization by the LI-COR Odyssey infrared imaging system (LI-COR). Details regarding the primary antibodies used are in the Supplemental Material. Uncropped Western blots are in Supplemental Data Set S5.

Cellular respiration

Cellular respiration was measured using a Seahorse XFe24 extracellular flux analyzer (Agilent) as described previously (Shao et al. 2016). See the Supplemental Material for additional details.

Statistics, reproducibility, and data availability

Statistical analysis was carried out as indicated in the figure legends. Exact *P*-values, sample sizes, and numbers of repetitions are in Supplemental Data Set S6. RNA-seq and ChIP-seq data have been deposited to Gene Expression Omnibus (accessions GSE165974, GSE169669, and GSE169672).

Competing interest statement

The authors declare no competing interests.

Acknowledgments

We thank C. Lee, the University of Texas Southwestern Animal Resource Center, Live Cell Imaging Core, Flow Cytometry Core, and McDermott Sequencing Center for excellent assistance with experiments performed here. This study and/or personnel were supported in part by National Institutes of Health National Institute of Diabetes and Digestive and Kidney Diseases R01 DK104789, R01 DK119163, and RC2 DK118620 to R.K.G., and 16POST26420136 and 19CDA34670007 from the American Heart Association and Harry S. Moss Heart Trust to M.S.

Author contributions: B.S., M.S., and R.K.G. conceived the study and wrote the manuscript. B.S., M.S., Y.A.A., and R.K.G. designed experiments. B.S., M.S., Q.Z., L.V., and Y.A.A, performed experiments. All authors analyzed the data.

References

Brestoff J, Kim B, Saenz S, Stine R, Monticelli L, Sonnenberg G, Thome J, Farber D, Lutfy K, Seale P, et al. 2015. Group 2 innate lymphoid cells promote beiging of white adipose tissue and limit obesity. *Nature* **519:** 242–246. doi:10.1038/nature14115

Burl R, Ramseyer V, Rondini E, Pique-Regi R, Lee Y, Granneman J. 2018. Deconstructing adipogenesis induced by β3-adrenergic receptor activation with single-cell expression profiling. *Cell Metab* **28:** 300–309.e4. doi:10.1016/j.cmet.2018.05.025

Cohen P, Kajimura S. 2021. The cellular and functional complexity of thermogenic fat. *Nat Rev Mol Cell Biol* **22:** 393–409. doi:10.1038/s41580-021-00350-0

Hepler C, Shan B, Zhang Q, Henry G, Shao M, Vishvanath L, Ghaben A, Mobley A, Strand D, Hon G, et al. 2018. Identification of functionally distinct fibro-inflammatory and adipogenic stromal subpopulations in visceral adipose tissue of adult mice. *Elife* **7:** e39636. doi:10.7554/eLife.39636

Lee M, Odegaard J, Mukundan L, Qiu Y, Molofsky A, Nussbaum J, Yun K, Locksley R, Chawla A. 2015. Activated type 2 innate lymphoid cells regulate beige fat biogenesis. *Cell* **160:** 74–87. doi:10.1016/j.cell.2014.12.011

Lončar D. 1991. Convertible adipose tissue in mice. *Cell Tissue Res* **266:** 149–161. doi:10.1007/BF00678721

Lüthi A, Cullen S, Mcneela E, Duriez P, Afonina I, Sheridan C, Brumatti G, Taylor R, Kersse K, Vandenabeele P, et al. 2009. Suppression of interleukin-33 bioactivity through proteolysis by apoptotic caspases. *Immunity* **31:** 84–98. doi:10.1016/j.immuni.2009.05.007

Mahlakõiv T, Flamar A, Johnston L, Moriyama S, Putzel G, Bryce P, Artis D. 2019. Stromal cells maintain immune cell homeostasis in adipose tissue via production of interleukin-33. *Sci Immunol* **4:** eaax0416. doi:10.1126/sciimmunol.aax0416

Mathis D. 2016. Il-33, imprimatur of adipocyte thermogenesis. *Cell* **166:** 794–795. doi:10.1016/j.cell.2016.07.051

Merrick D, Sakers A, Irgebay Z, Okada C, Calvert C, Morley M, Percec I, Seale P. 2019. Identification of a mesenchymal progenitor cell hierarchy in adipose tissue. *Science* **364:** eaav2501. doi:10.1126/science.aav2501

Molofsky A, Savage A, Locksley R. 2015. Interleukin-33 in tissue homeostasis, injury, and inflammation. *Immunity* **42:** 1005–1019. doi:10.1016/j.immuni.2015.06.006

Odegaard J, Lee M, Sogawa Y, Bertholet A, Locksley R, Weinberg D, Kirichok Y, Deo R, Chawla A. 2016. Perinatal licensing of thermogenesis by Il-33 and St2. *Cell* **166:** 841–854. doi:10.1016/j.cell.2016.06.040

Qiu Y, Nguyen K, Odegaard J, Cui X, Tian X, Locksley R, Palmiter R, Chawla A. 2014. Eosinophils and type 2 cytokine signaling in macrophages orchestrate development of functional beige fat. *Cell* **157:** 1292–1308. doi:10.1016/j.cell.2014.03.066

Rana B, Jou E, Barlow J, Rodriguez-Rodriguez N, Walker J, Knox C, Jolin H, Hardman C, Sivasubramaniam M, Szeto A, et al. 2019. A stromal cell niche sustains Ilc2-mediated type-2 conditioning in adipose tissue. *J Exp Med* **216:** 1999–2009. doi:10.1084/jem.20190689

Schwalie P, Dong H, Zachara M, Russeil J, Alpern D, Akchiche N, Caprara C, Sun W, Schlaudraff K, Soldati G, et al. 2018. A stromal cell population that inhibits adipogenesis in mammalian fat depots. *Nature* **559:** 103–108. doi:10.1038/s41586-018-0226-8

Shamsi F, Tseng Y, Kahn C. 2021. Adipocyte microenvironment: everybody in the neighborhood talks about the temperature. *Cell Metab* **33:** 4–6. doi:10.1016/j.cmet.2020.12.012

Shan B, Shao M, Zhang Q, Hepler C, Paschoal V, Barnes S, Vishvanath L, An Y, Jia L, Malladi V, et al. 2020. Perivascular mesenchymal cells control adipose-tissue macrophage accrual in obesity. *Nat Metab* **2:** 1332–1349. doi:10.1038/s42255-020-00301-7

Shao M, Ishibashi J, Kusminski C, Wang Q, Hepler C, Vishvanath L, Macpherson K, Spurgin S, Sun K, Holland W, et al. 2016. Zfp423 maintains white adipocyte identity through suppression of the beige cell thermogenic gene program. *Cell Metab* **23:** 1167–1184. doi:10.1016/j.cmet.2016.04.023

Shao M, Vishvanath L, Busbuso N, Hepler C, Shan B, Sharma A, Chen S, Yu X, An Y, Zhu Y, et al. 2018. De novo adipocyte differentiation from Pdgfrβ$^+$ preadipocytes protects against pathologic visceral adipose expansion in obesity. *Nat Commun* **9:** 890. doi:10.1038/s41467-018-03196-x

Shao M, Hepler C, Zhang Q, Shan B, Vishvanath L, Henry G, Zhao S, An Y, Wu Y, Strand D, et al. 2021. Pathologic Hif1α signaling drives adipose progenitor dysfunction in obesity. *Cell Stem Cell* **28:** 685–701.e7. doi:10.1016/j.stem.2020.12.008

Spallanzani R, Zemmour D, Xiao T, Jayewickreme T, Li C, Bryce P, Benoist C, Mathis D. 2019. Distinct immunocyte-promoting and adipocyte-generating stromal components coordinate adipose tissue immune and metabolic tenors. *Sci Immunol* **4:** eaaw3658. doi:10.1126/sciimmunol.aaw3658

Vishvanath L, Macpherson K, Hepler C, Wang Q, Shao M, Spurgin S, Wang M, Kusminski C, Morley T, Gupta R. 2016. Pdgfrβ$^+$ mural preadipocytes contribute to adipocyte hyperplasia induced by high-Fat-diet feeding and prolonged cold exposure in adult mice. *Cell Metab* **23:** 350–359. doi:10.1016/j.cmet.2015.10.018